

Article

Qualitative Analysis of the Heat Transfer in a Package of Square Steel Sections

Rafał Wyczółkowski ¹, Vazgen Bagdasaryan ^{2,*}, Suren G. Aghbalyan ³, Gayane A. Vasilyan ³ and Marek Gała ⁴

¹ Department of Production Management, Czestochowa University of Technology, Armii Krajowej 19, 42-200 Czestochowa, Poland; rafal.wyczolkowski@pcz.pl

² Institute of Civil Engineering, Warsaw University of Life Sciences—SGGW, Nowoursynowska 166, 02-787 Warsaw, Poland

³ Faculty of Mining and Metallurgy, National Polytechnic University of Armenia, Teryan 105, Yerevan 0009, Armenia; metalsur@polytechnic.am (S.G.A.); gayavasi@gmail.com (G.A.V.)

⁴ Institute of Electric Power Engineering, Czestochowa University of Technology, Armii Krajowej 17, 42-200 Czestochowa, Poland; marek.gala@pcz.pl

* Correspondence: vazgen_bagdasaryan@sggw.edu.pl

Abstract: During the heat treatment of square or rectangular steel sections, a heated charge, arranged in regular packages, is placed inside a furnace. This type of charge forms a porous medium through which a complex heat flow occurs during heating. Several heat transfer mechanisms act simultaneously within this medium: conduction through the section walls, conduction and natural convection within the gas, thermal radiation between the section walls, and complex heat transfer (mainly contact conduction) at the joints between the adjacent sections. This article presents a qualitative analysis of heat transfer, aiming to determine the contribution of individual heat transfer mechanisms to the overall process. For this purpose, an analytical model of complex heat transfer within the package was employed, based on the thermo-electric analogy. The results from experimental studies were used to calculate the natural convection and heat transfer at the joints. It was assumed that the material of the sections was low-carbon steel, and the gas was air. Calculations were performed for the temperature range of 25 °C to 700 °C, considering three different geometrical configurations of the sections. It was shown that the effective thermal conductivity (ETC) of the package for the considered geometrical cases varies between 2.2 and 10.6 W/(m·K), which is an order of magnitude lower than the thermal conductivity of the individual sections. This parameter increased dynamically with the temperature. Moreover, the heat transfer intensity within the package of sections was nearly an order of magnitude lower than the heat conduction observed in a solid steel charge. Additionally, it was shown that the primary heat transfer mechanisms governing the heating process were thermal conduction (in the lower temperature range—up to approximately 350 °C) and thermal radiation (in the higher temperature range—above 350 °C). The gas convection inside the sections had a minimal impact on the heating process of the package. The primary parameters influencing the quality of the results were the joint resistance between the adjacent sections and the emissivity of the sections. The presented model can be used for the optimization of heat treatment processes for the considered charge.

Keywords: steel section; heat treatment; complex heat transfer; thermo-electric analogy; thermal resistance



Citation: Wyczółkowski, R.; Bagdasaryan, V.; Aghbalyan, S.G.; Vasilyan, G.A.; Gała, M. Qualitative Analysis of the Heat Transfer in a Package of Square Steel Sections. *Materials* **2024**, *17*, 5412. <https://doi.org/10.3390/ma17225412>

Academic Editor: Andrea Di Schino

Received: 8 October 2024

Revised: 27 October 2024

Accepted: 4 November 2024

Published: 6 November 2024



Copyright: © 2024 by the authors. Licensee MDPI, Basel, Switzerland. This article is an open access article distributed under the terms and conditions of the Creative Commons Attribution (CC BY) license (<https://creativecommons.org/licenses/by/4.0/>).

1. Introduction

In response to the climate crisis, manifesting itself as global warming, various industrial sectors are actively developing technologies aimed at reducing energy consumption and greenhouse gas emissions [1–6]. This challenge also affects the metallurgical sector, particularly in the heat treatment of steel products [7–11]. Additionally, industrial heat treatment operations significantly impact production efficiency and the quality of finished products. For this reason, ongoing research addresses various aspects of the heat treatment

of steel products [12–17]. These challenges make it essential to optimize such processes. It should be emphasized that this optimization should occur both at the process design stage and during its execution on the production line. Today, for efficient process design and control, specialized numerical models are employed, capable of predicting spatial and temporal temperature changes in the treated charge. Such models have been successfully used in the metallurgical industry for over four decades [18–20]. One of the crucial parameters for the accurate operation of these models is the thermal properties of the heated charge. When analyzing the heating process of monolithic steel elements, the primary thermal property is the thermal conductivity of steel. This task becomes especially challenging when dealing with a porous structure within the treated charge [21–23]. An example of such a charge is a package of square or rectangular steel sections (Figure 1). The inhomogeneous, two-phase structure (steel–gas) of these elements leads to complex heat flow dynamics, arising from the simultaneous occurrence of heat conduction, natural convection, and thermal radiation. For this reason, the thermal property essential for optimizing heat treatment is not the thermal conductivity of steel itself. Instead, the effective thermal conductivity (ETC or k_{ef}), as the primary thermal property of section bundles, should be considered. This parameter is widely used in studies of porous media [24–26]. By employing effective thermal conductivity, it becomes possible to describe transient heat transfer within a porous charge and to determine its heating time [23,27,28], which is crucial for optimizing heat treatment processes.

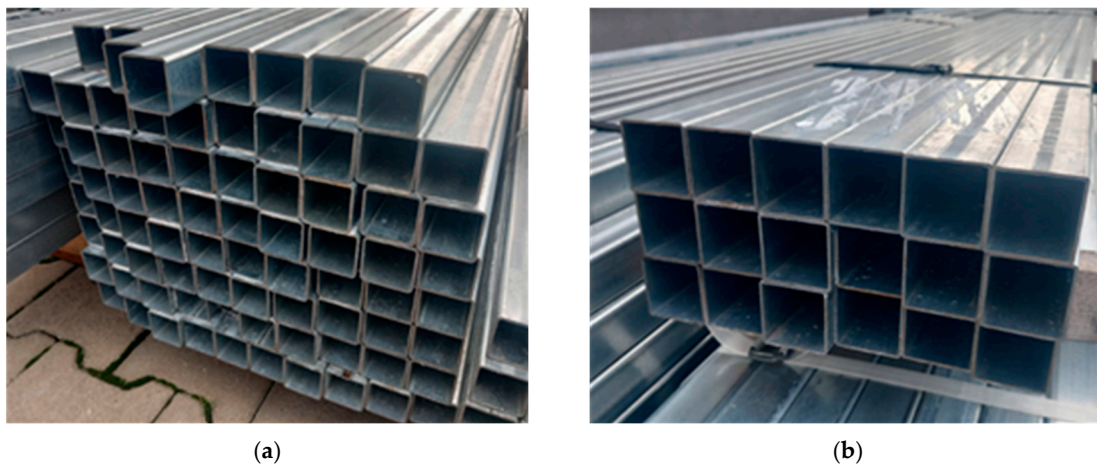


Figure 1. Packages of steel square sections prepared for heat treatment. (a) sections 60 mm; (b) sections 80 mm.

The most reliable method for determining effective thermal conductivity is through experimental investigations. For cellular and porous materials, this is typically measured using the steady-state method with a guarded hot plate apparatus [29,30]. However, this approach requires specialized equipment, is time-consuming, and involves preparing specific test samples. A major limitation of these measurements is that the results are not universally applicable, as they are specific to individual material samples. Consequently, model calculations are often used as an effective alternative for determining the ETC of porous materials [25].

Various analytical models for estimating the effective thermal conductivity of two-phase media (solid–gas) are available in the literature. The most commonly used ETC models include the following: parallel and series models [31], Effective Medium Theory (EMT) [32], Maxwell–Eucken [32], Horai [33], Beck [34], Krischer [35], Woodside–Messmer [36], Assad [37], and Bruggeman [38]. However, as demonstrated in our calculations, these models are not suitable for determining the ETC of section bundles [39]. This limitation arises because these models do not account for the specific heat transfer

mechanisms occurring during the heating of the charge in question, particularly contact conduction and thermal radiation.

This article presents a mathematical model for the effective thermal conductivity of a package of square steel sections. It is an empirical model because the relationships describing thermophysical parameters—such as the thermal conductivity of steel and gas, the Nusselt number, and joint resistance—were determined based on the approximation of experimental data. The results of these studies have been detailed in previous publications by authors [40–43]. This model is relatively simple yet provides a comprehensive description of the complex heat transfer phenomena occurring within the package of sections.

The greatest scientific contribution of the presented research lies in demonstrating that, thanks to the developed computational model, it is possible to quantitatively and qualitatively analyze the highly complex physical phenomenon of heat transfer using relatively simple mathematical relationships. The primary scientific objective of this article is to illustrate to what extent the heating process of a package of sections differs from the heating of solid steel elements, and to identify which heat transfer mechanisms primarily determine its intensity.

2. Materials and Methods

The presented model is based on the analysis of thermal resistances associated with individual heat transfer mechanisms occurring during the heating of the considered medium. This approach relies on the analogy between electrical and thermal conduction phenomena, stemming from the similarity in the mathematical expressions of Ohm's and Fourier's laws [44]. In many cases, this method provides an effective alternative for addressing complex heat transfer problems in heterogeneous systems, offering a simpler solution than more complex numerical methods [45–52].

The starting point for deriving the appropriate mathematical relationships that describe the phenomenon of complex heat flow was the physical model of the medium under consideration. As shown in Figure 2, this model consists of a packed, layered bed of square sections, within which unidirectional, steady heat flow occurs. Due to this assumption, thermal energy in this system is transferred alternately through the layers of sections and the joints between them.

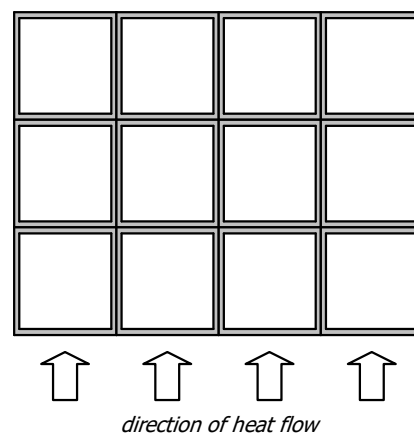


Figure 2. The physical model of the system under consideration in the form of a layered, packed bed of square sections with a steady, unidirectional heat flow.

The value of ETC for the considered medium was calculated using the definition of thermal resistance to conduction through the plane wall [53]:

$$ETC = \frac{\delta_c}{R_{to}}, \quad (1)$$

where R_{t0} and δ_c are the total thermal resistance and characteristic dimension of the considered medium, respectively. Since the width of the joints was on the order of hundredths of a millimeter, it was assumed that the parameter δ_c corresponded to the external dimension of the sections.

The total thermal resistance of the considered bed was a serial connection of section thermal resistance R_{st} and joint thermal resistance R_j :

$$R_{t0} = R_{st} + R_j, \tag{2}$$

In order to determine the resistance R_{st} , it was necessary to take into consideration the following phenomena of heat transfer: conduction in steel walls, conduction and free convection within gas (these two phenomena were analyzed jointly) and the thermal radiation between the inner surfaces of a section. Each of the mentioned mechanisms was assigned a corresponding thermal resistance, i.e., thermal resistance in steel, thermal resistance in gas R_{gs} and radiation resistance R_{rd} .

Since the actual, multidimensional phenomenon of heat transfer was treated here as one-dimensional, obtaining a solution required two assumptions: (a) any plane wall normal to the direction of heat flow was isothermal, and (b) any plane parallel to the direction of heat flow was adiabatic [44]. This led to two separate resistance networks, resulting in two different total thermal resistances denoted as R_{st-a} and R_{st-b} . The resistance R_{st-a} corresponded to the division of the section into three vertical zones I–III, parallel to the direction of heat flow, as shown in Figure 3a. The resistance R_{st-b} corresponded to the division of the section into three horizontal layers 1–3 (Figure 3b). The thermal resistance networks corresponding to the different section divisions are presented in Figure 4.

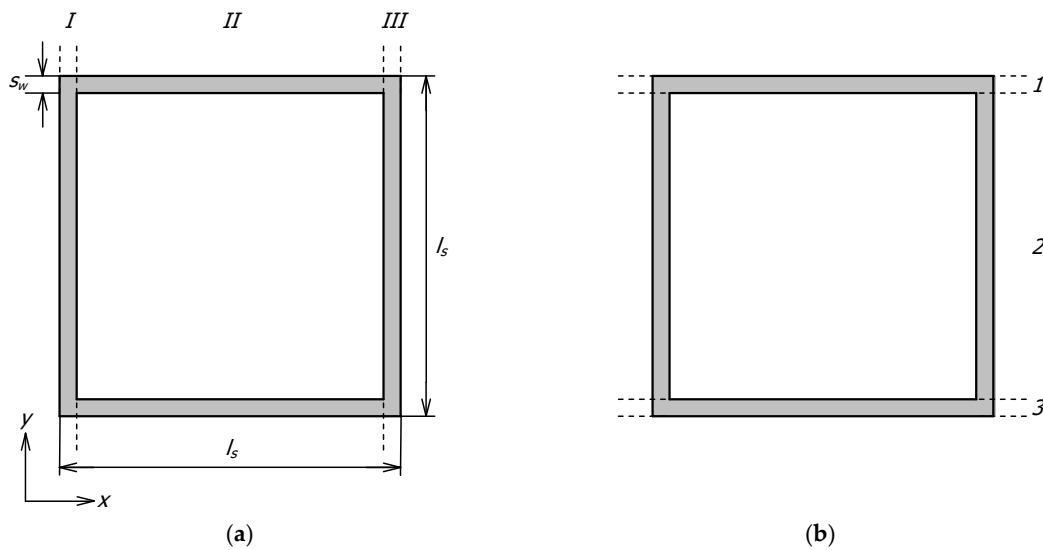


Figure 3. Division of a section into: (a) vertical zones I–III, (b) horizontal layers 1–3.

Taking into account the adopted assumptions, the resistances R_{st-a} and R_{st-b} could be described using the following relationships:

$$R_{st-a} = \left(\frac{1}{R_I} + \frac{1}{R_{II-1} + \left(\frac{1}{R_{gs}} + \frac{1}{R_{rd}} \right)^{-1} + R_{II-3}} + \frac{1}{R_{III}} \right)^{-1}, \tag{3}$$

$$R_{st-b} = R_1 + \left(\frac{1}{R_{2-I}} + \frac{1}{R_{gs}} + \frac{1}{R_{rd}} + \frac{1}{R_{2-III}} \right)^{-1} + R_3 \tag{4}$$

The final value of the R_{st} was calculated using the following formula [54]:

$$R_{st} = \frac{R_{st-a} + 2R_{st-b}}{3}, \tag{5}$$

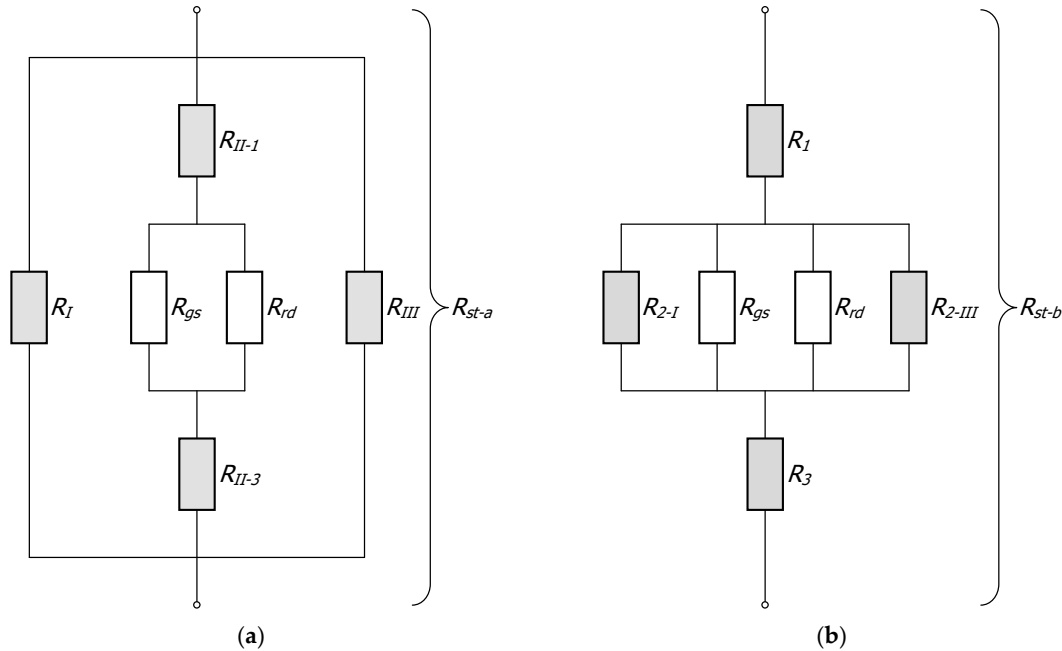


Figure 4. Thermal resistance networks of a square section: (a) network for resistance R_{st-a} , (b) network for resistance R_{st-b} .

The resistances from Equations (3) and (4), which relate to conduction in section walls (they were marked gray in Figure 4), were described with the following relationships:

$$R_I = R_{III} = \frac{l_s}{k_s \cdot f_I}, \tag{6}$$

$$R_{II-1} = R_{II-3} = \frac{s_w}{k_s \cdot f_{II}} \tag{7}$$

$$R_1 = R_3 = \frac{s_w}{k_s} \tag{8}$$

$$R_{2-I} = R_{2-III} = \frac{(l_s - 2s_w)}{k_s \cdot f_I} \tag{9}$$

where l_s is the external dimension of the section, s_w is the wall thickness of the section, k_s is the thermal conductivity of steel, and f_I, f_{II} and f_{III} are the relative surface areas of the respective zones:

$$f_I = f_{III} = \frac{s_w}{l_s}, \tag{10}$$

$$f_{II} = \frac{l_s - 2s_w}{l_s} \tag{11}$$

The resistance R_{gs} pertains to the heat transfer processes in the internal area of the section that is filled with gas. These processes include heat conduction and free convection. In the adopted solution, both phenomena were treated jointly as an intensified conduction, expressed quantitatively by the equivalent gas thermal conductivity k_{eq} [44]:

$$k_{eg} = Nu \cdot k_g, \tag{12}$$

where Nu is the Nusselt number and k_g is the thermal conductivity of gas.

The internal spaces of the sections were treated as horizontal enclosures. For this type of geometry, the Nusselt number was calculated using the criterial relationship with the Rayleigh number Ra [54]:

$$Nu = C \cdot Ra^m, \quad (13)$$

where the constants C and m depended on the Rayleigh number Ra (the values of C and m used are listed in Table 1).

Table 1. Values of the constants C and m in relation to the Rayleigh number Ra [27].

Rayleigh Number Ra	C	m
$10^4 < Ra < 4 \times 10^5$	0.195	0.25
$4 \times 10^5 < Ra < 10^7$	0.068	0.33

Based on the research described in [42,43], for calculating the temperature change in the Nusselt number for square sections (60 mm and 80 mm), the following relationships were established:

$$Nu_{60} = 4.3 \cdot 10^{-13}t^5 - 7.9 \cdot 10^{-10}t^4 + 6.1 \cdot 10^{-7}t^3 - 2.11 \cdot 10^{-4}t^2 + 0.027t + 2.6, \quad (14)$$

$$Nu_{80} = 6.1 \cdot 10^{-13}t^5 - 1.3 \cdot 10^{-9}t^4 + 1.05 \cdot 10^{-6}t^3 - 3.96 \cdot 10^{-4}t^2 + 0.056t + 4.2 \quad (15)$$

As demonstrated in the referenced studies, for sections smaller than 60 mm, the Nusselt number did not exceed the value of 1.2. Therefore, for such sections, the phenomenon of free convection was neglected. Ultimately, the resistance R_{gs} was described by the formula:

$$R_{gs} = \frac{(l_s - 2s_w)}{Nu \cdot k_g \cdot f_{II}}, \quad (16)$$

Radiation resistance R_{rd} was solved through analysis of the radiosity balance of flat surfaces in the square cavity that closed a space [55]. The methodology for the determination of resistance R_{rd} for such geometry was described in [56]. When the temperature difference ΔT in the system was much smaller than its mean absolute temperature T , radiation resistance could be described by:

$$R_{rd} = \frac{1}{\varepsilon} \cdot \frac{1}{4\sigma_c T^3}, \quad (17)$$

where σ_c is the Stefan–Boltzmann constant and ε is the emissivity of the section surface.

According to Equation (2), the intensity of heat flow in the section package also depended on the joint thermal resistance R_j . Due to the shape inaccuracies of the sections, contact between the adjacent layers did not occur across the entire surface of the package, but only on small discrete contour areas whose geometry was entirely random. For this reason, the resistance R_j could not be described by commonly used analytical relationships [57–60]. Furthermore, experimental investigations of this parameter are also challenging due to the hollow interior of the sections, which complicates the measurement of temperature distribution along those elements. To overcome this problem, it was assumed that the joint resistance in this case was similar to the joint resistance in a bed of rectangular steel bars. As established through experimental measurements using a guarded hot plate apparatus, the joint resistance for this type of medium decreased with increasing temperature [40]. Moreover, the variability of many physical factors characterizing the discussed joints caused the resistance R_j at a given temperature to take on values within a

certain range. The minimum and maximum values of the resistance R_j in the function of temperature could be described by the following formulas:

$$R_{j-\min} = \left(1.25 \cdot 10^{-5} t^2 - 0.0288 t + 32.91\right) \cdot 10^{-4}, \quad (18)$$

$$R_{j-\max} = \left(2.31 \cdot 10^{-5} t^2 - 0.0534 t + 58.16\right) \cdot 10^{-4} \quad (19)$$

As indicated by Equations (18) and (19), in the temperature range of 25 to 700 °C, the value of $R_{j-\max}$ constituted approximately 180% to 143% of the value of $R_{j-\min}$.

It should be noted that the proposed model also allowed for the analysis of heat transfer in a package of rectangular profiles. In this case, instead of a single profile dimension l_s , two dimensions must be provided (width l_x and height l_y). For rectangular geometry, the equations involving the l_s parameter, as well as Equation (17), which described radiation resistance, were slightly modified. For rectangular geometry, this equation takes the form:

$$R_{rd} = \frac{\left((2l_x - 4s_w) \cdot \frac{1}{\epsilon}\right) + l_y - l_x}{(l_x + l_y - 4s_w)} \cdot \frac{1}{4\sigma_c T^3}. \quad (20)$$

The first term on the right side of the above equation results from the algebra of view factors [56]. When the profile is square ($l_x = l_y = l_s$), the above equation simplifies to form (17).

In summary, discussing the proposed mathematical model, it is important to emphasize that it describes the entire spectrum of thermal phenomena occurring during the heating of a package of sections, while also accounting for the variation in their intensity with increasing or decreasing temperature. It should also be noted that the originality of this model lies in the use of empirical equations, the forms of which the authors developed based on their own experimental research (Equations (14), (15), (18) and (19)) or by approximating the literature data (Equations (20) and (21)). As a result, it served as a highly versatile computational tool, enabling both quantitative and qualitative analyses of the heat transfer process within the package of steel sections. Furthermore, due to the simplicity of the mathematical relationships employed, calculations could be performed using standard spreadsheet software. To perform the calculations, the authors implemented this model in Scilab (version 6.0.1), a free and open-source software for engineers and scientists available under the GPL License. More information about this software can be found on the following website: <https://www.scilab.org> (accessed on 25 October 2024).

3. Results and Discussion

The analyses presented below pertain to heat transfer phenomena in a package of square profiles during annealing. This type of heat treatment aims to alter the structure of steel and its mechanical properties. In the case of carbon steel, annealing serves to reduce hardness, improve ductility, eliminate internal stresses, and homogenize the material structure. The temperature at which these processes occur depends on the type of annealing and the carbon content in the steel [61]. For example, softening annealing is conducted at temperatures between 650 and 750 °C (below the critical temperature of steel) and aims to reduce hardness, facilitating further mechanical processing. Stress-relief annealing occurs at lower temperatures, typically between 550 and 650 °C, and aims to reduce internal stresses that may have developed due to previous mechanical or thermal processing. The steel is slowly cooled after being heated to this temperature. It is important to note that the exact annealing temperature depends on the carbon content of the steel. Steel with a higher carbon content (e.g., high-carbon steel) will have higher austenitizing temperatures compared to low-carbon steel. All the calculations were conducted for a temperature range of 25 to 700 °C. As indicated by the information provided above, this is the typical temperature range encountered during the annealing of carbon steel products.

In the calculations, the following parameters were used as the input data: section size l_s , section wall thickness s_w , section surface emissivity ε (assumed $\varepsilon = 0.7$), Nusselt number Nu , joint thermal resistance (minimum R_{j-min} and maximum R_{j-max}), and the thermal conductivities of steel k_s and gas k_g . It was considered that the thermophysical parameters Nu , R_j , k_s , and k_g vary with temperature. Changes in the thermal conductivity of steel over the temperature range of 25 to 700 °C were described by the following equation [62]:

$$k_s = 112.51x_c^2 - 100.85x_c + 68.89 - (0.42x_c^2 + 0.318x_c + 0.065)t + (334.05x_c^2 - 247.27x_c + 18.59) \cdot 10^{-6}t^2, \quad (21)$$

where x_c means the percentage of carbon in the steel (it was assumed $x_c = 0.2\%$).

In performing the calculations, it was assumed that the gas filling the interior of the sections was air. The equation describing the changes in the thermal conductivity of air over the temperature range of 25 to 700 °C was derived by approximating tabulated data [63]:

$$k_{g-air} = -2.88 \cdot 10^{-8}t^2 + 8.05 \cdot 10^{-5}t + 0.024, \quad (22)$$

Model calculations illustrating various aspects of the heat transfer phenomenon within the package of sections were performed for nine geometric cases. Three section sizes l_s were considered: 40 mm, 60 mm, and 80 mm. For each section, three wall thicknesses s_w were taken into account: 1 mm, 2 mm, and 3 mm for the 40 mm section, and 2 mm, 3 mm, and 4 mm for the 60 mm and 80 mm sections. Additionally, for each case, calculations were performed for both the minimum and maximum values of the joint resistance R_j . In the first case, the maximum values of the effective thermal conductivity (ETC) were obtained (ETC^{max}), while in the second case, the minimum values were obtained (ETC^{min}).

Firstly, the results of the calculations of effective thermal conductivity (ETC) for the case of complete heat exchange, when all the possible mechanisms of this phenomenon (conduction, free convection, and radiation) occurred, are shown. These results, in the form of graphs showing changes in the considered parameter as a function of temperature, were divided according to the various section sizes and are presented in Figures 5–7. The graphs labeled (a) show the maximum values of ETC, while the graphs labeled (b) show the minimum values. Each graph presents three series of results referring to different wall thicknesses of the section. As evident from the provided graphs, the analyzed parameter increased as a function of the temperature in every case. This trend was attributed to the phenomenon of thermal radiation, the intensity of which was proportional to the third power of the absolute temperature. The increase in ETC also occurred with larger section dimensions and greater wall thickness. The first effect was caused by the interplay of many factors, with thermal radiation having the most significant influence. The second effect arose from the increased contribution of heat conduction through the walls of the sections. Given that steel is a good conductor of heat, this mode of heat transfer was the most effective mechanism for transferring energy within the examined charge.

The results of the calculations presented in the graphical form primarily demonstrated the qualitative nature of the changes in the ETC parameter. However, to better convey the computational data in a quantitative sense, they were also presented in a tabular form (Table 2), where for each computational case, the minimum, average, and maximum values of the ETC were compiled.

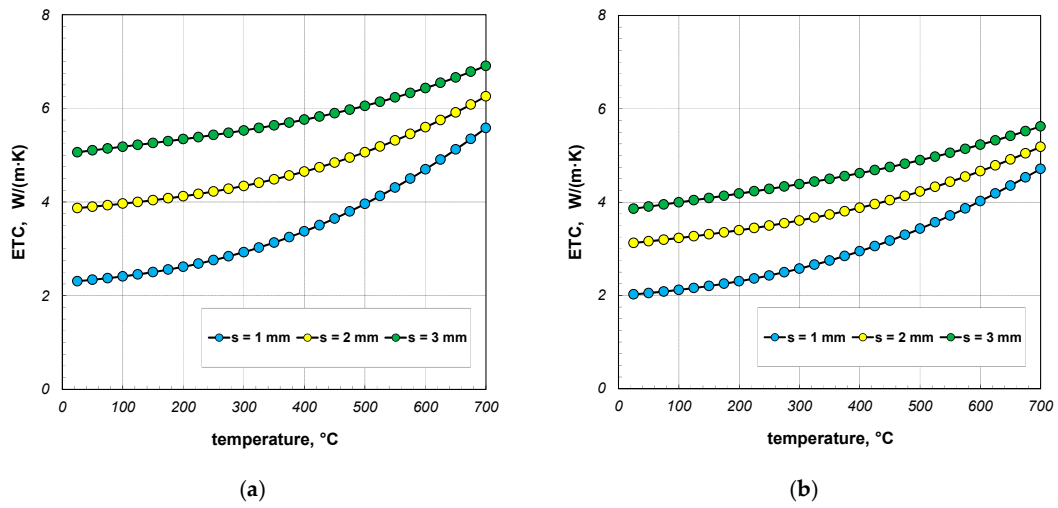


Figure 5. ETC of the 40 mm section package for the (a) minimum and (b) maximum joint resistance.

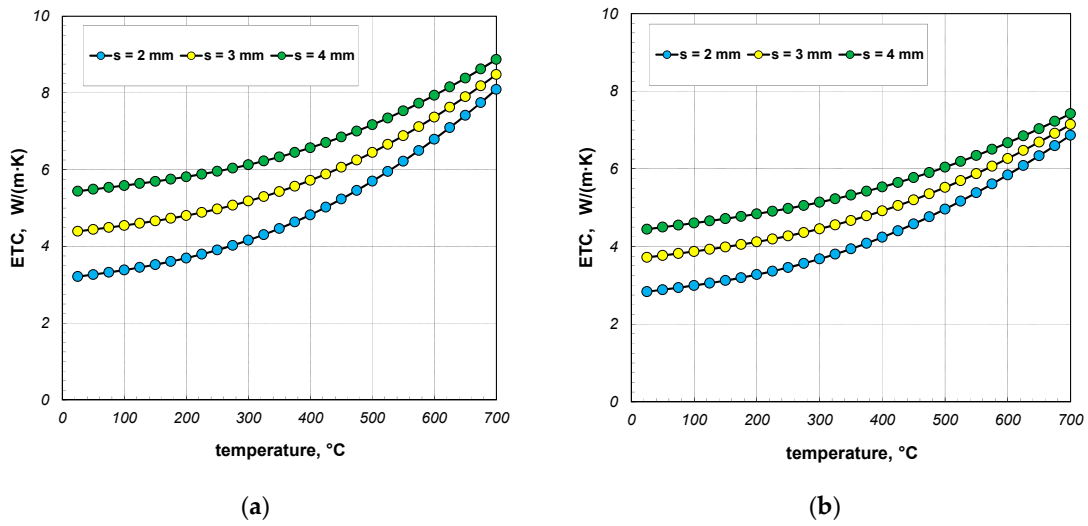


Figure 6. ETC of the 60 mm section package for the (a) minimum and (b) maximum joint resistance.

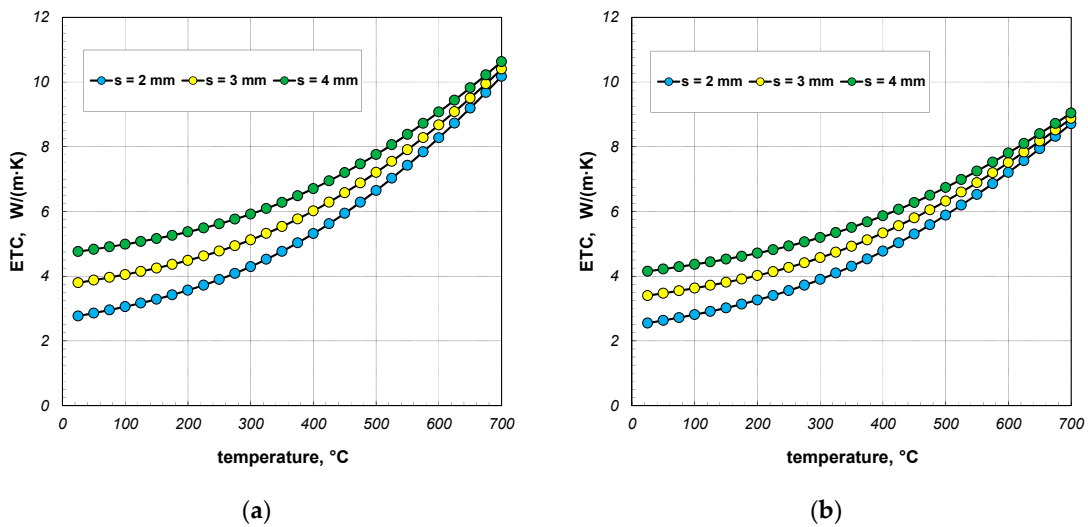


Figure 7. ETC of the 80 mm section package for the (a) minimum and (b) maximum joint resistance.

Table 2. The minimum, average, and maximum values of ETC.

Section Size	Wall Thickness	ETC, W/(m·K)					
		R_{j-min}			R_{j-max}		
		Min	Mean	Max	Min	Mean	Max
40 mm	1 mm	2.31	3.47	5.58	2.02	3.01	4.71
	2 mm	3.87	4.72	6.26	3.12	3.91	5.18
	3 mm	5.06	5.71	6.91	3.85	4.61	5.62
60 mm	2 mm	3.21	4.96	8.09	2.83	4.32	6.86
	3 mm	4.39	5.84	8.48	3.72	4.99	7.14
	4 mm	5.44	6.67	8.87	4.44	5.58	7.42
80 mm	2 mm	2.77	5.48	10.18	2.55	4.87	8.71
	3 mm	3.80	6.19	10.40	3.39	5.44	8.87
	4 mm	4.76	6.87	10.63	4.15	5.97	9.04

As indicated by the results presented above, increasing the external dimension of the profiles l_s and the thickness of their walls s_w led to a rise in the value of the effective thermal conductivity (ETC). An increase in the parameter l_s resulted in fewer joints per unit length of the bundle, which corresponded to the unit of the ETC. These joints represented the areas of highest thermal resistance. Therefore, if the increase in l_s reduced the number of joints, the overall thermal resistance of the medium decreased, thereby increasing the value of the ETC. Conversely, increasing the wall thickness enhanced the area for heat conduction in the steel, which increased the parameters f_I and f_{III} , consequently reducing the thermal resistances R_I and R_{III} described by Equation (6).

A significant issue in analyzing heat flow within the package of sections was to decipher to what extent the value of the ETC differed from the thermal conductivity of the steel from which the sections were made. The difference between these two parameters straightforwardly indicated how quantitatively the heat transfer process in the package deviated from the simple heat conduction in solid steel. This discrepancy was illustrated using a parameter called the reduced effective thermal conductivity R_{ETC} , which is defined as the following product:

$$R_{ETC} = \frac{ETC}{k_s}, \quad (23)$$

The results of the calculations for the R_{ETC} parameter, presented in the form of graphs for each case of the analyzed charge, are shown in Figures 8–10. As seen, the R_{ETC} parameter increased significantly as a function of the temperature. The same effect was observed with the increasing section dimensions and wall thickness. Generally, for all the cases of the charge, the value of R_{ETC} ranged from 0.04 to 0.34, with an average value of approximately 0.15. This value indicates that the intensity of heat flow in the package of sections was nearly an order of magnitude lower than that of the conduction in steel (in the walls of the sections). This highlights how distinct the physical process of heating a package of sections, which is a porous granular material, is compared to the heating of solid steel charges. As with the ETC, for each computational case, Table 3 presents the minimum, average, and maximum values of R_{ETC} .

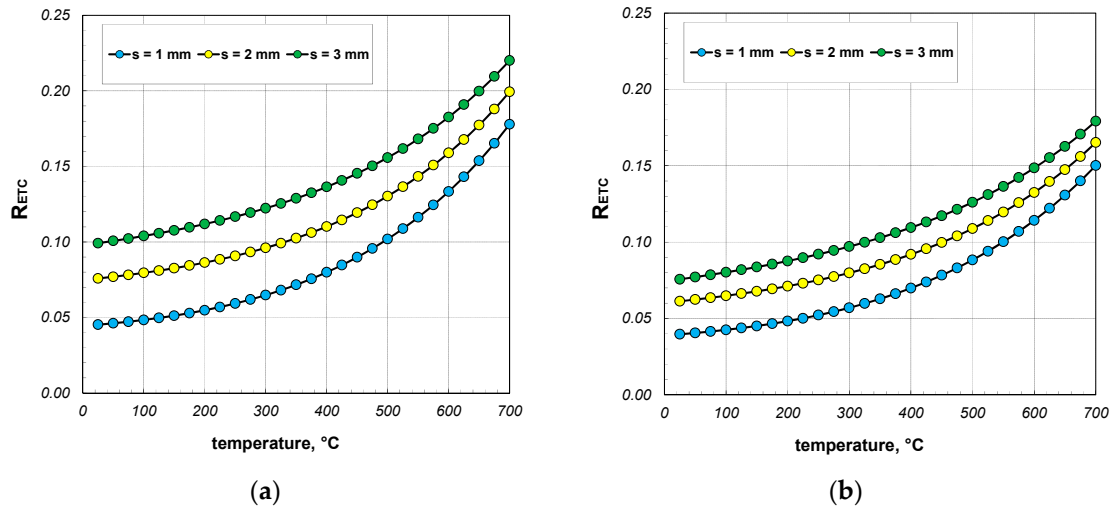


Figure 8. R_{ETC} of the 40 mm section package for the (a) minimum and (b) maximum joint resistance.

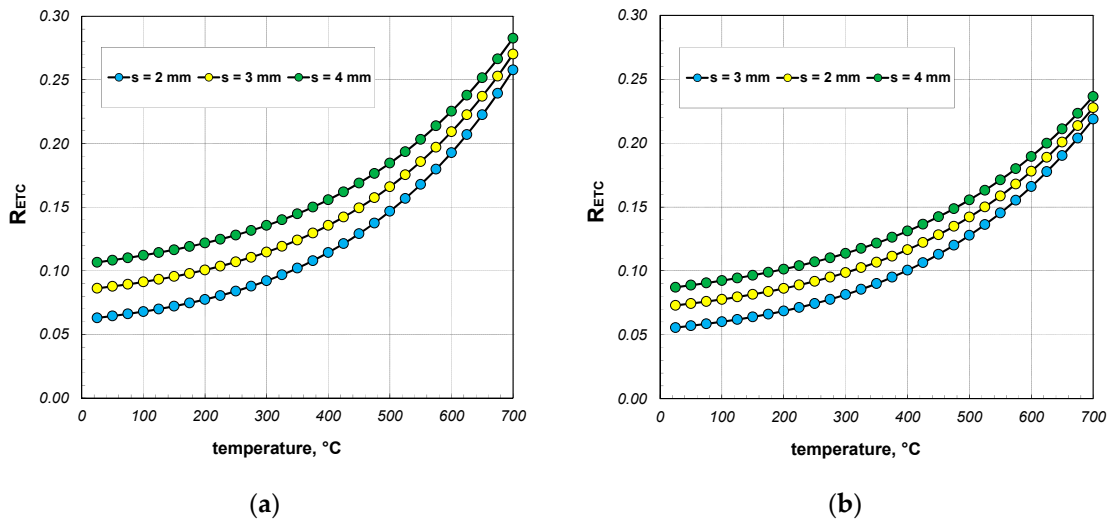


Figure 9. R_{ETC} of the 60 mm section package for the (a) minimum and (b) maximum joint resistance.

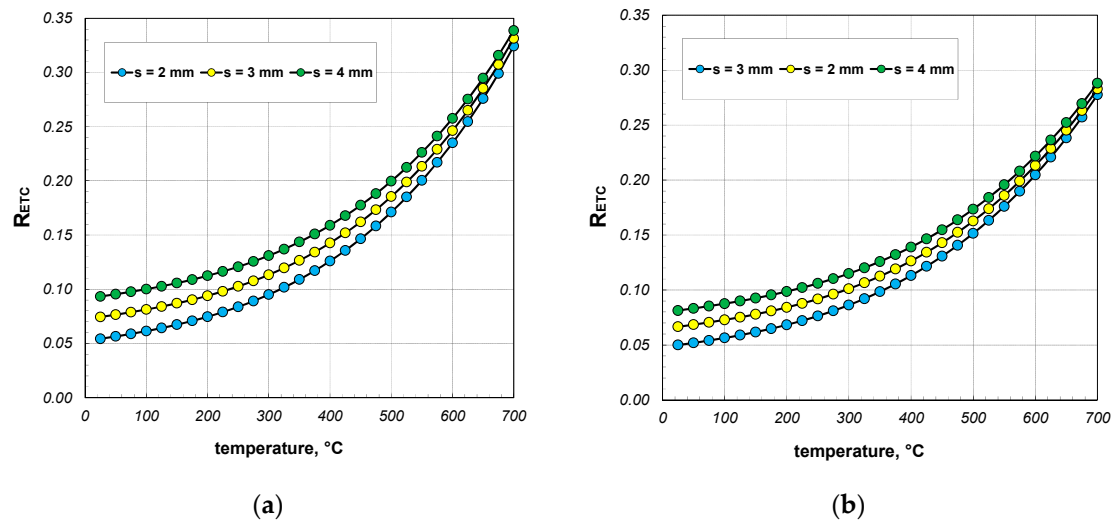


Figure 10. R_{ETC} of the 80 mm section package for the (a) minimum and (b) maximum joint resistance.

Table 3. The minimum, average, and maximum values of R_{ETC} parameter.

Section Dimension	Wall Thickness	R_{ETC}					
		R_{gp-min}			R_{gp-max}		
		Min	Mean	Max	Min	Mean	Max
40 mm	1 mm	0.045	0.087	0.178	0.039	0.075	0.150
	2 mm	0.076	0.116	0.199	0.061	0.096	0.165
	3 mm	0.099	0.141	0.220	0.075	0.112	0.179
60 mm	2 mm	0.063	0.124	0.257	0.056	0.108	0.219
	3 mm	0.086	0.144	0.271	0.073	0.123	0.227
	4 mm	0.106	0.163	0.283	0.087	0.137	0.236
80 mm	2 mm	0.054	0.139	0.324	0.049	0.124	0.278
	3 mm	0.074	0.156	0.331	0.067	0.136	0.283
	4 mm	0.093	0.171	0.339	0.081	0.148	0.288

The results presented in the following sections of the article pertain to the qualitative analysis of the heat transfer process within the package of sections. First, the aim was to determine the impact of the heat transfer phenomena occurring in the gas filling the interiors of the sections. As previously mentioned, these phenomena include conduction and free convection. To analyze this problem, a parameter denoted as MG_{ETC} was utilized, which is defined as the following quotient:

$$MG_{ETC} = \frac{ETC - ETC_{WG}}{ETC_{WG}}, \quad (24)$$

where ETC_{WG} denotes the effective thermal conductivity of the package calculated by excluding the heat transfer phenomena occurring in the gas region. The value of ETC_{WG} was obtained by omitting the resistance R_{gs} in the computational model.

The results of the MG_{ETC} parameter calculations are presented in Figures 11–13. When discussing these data, it is important to note that the free convection of air in enclosures is highly dependent on their geometry (dimensions and shape). In this analyzed case, these enclosures were horizontal channels with a square cross-section. As determined by our own research, convection was practically non-existent in the 40 mm sections [41,42]. Therefore, it was assumed that for this package of sections, the Nusselt number was constant and took a value of 1.2. For the packages of the 60 mm and 80 mm sections, the Nusselt number was calculated using Equations (14) and (15). As a result, the changes in the MG_{ETC} parameter obtained for the various packages were highly varied. In the case of the 40 mm section package (Figure 11), where free convection was negligible, the analyzed parameter increased as a function of the temperature. This trend in the results was attributed to the changes in the thermal conductivity of both the steel and the air. Within the analyzed temperature range, the coefficient k_s decreased from 50.1 to 29.4 W/(m·K), while k_g increased from 0.026 to 0.061 W/(m·K). The MG_{ETC} parameter decreased significantly with the increasing wall thickness of the section. In summary, it can be stated that for the 40 mm section package, the heat transfer phenomena in the gas accounted for a maximum of 4% of the energy transfer, with an average value of approximately 1%.

A different trend in the MG_{ETC} parameter was observed for the packages of the 60 mm and 80 mm sections. In this case, the free convection of air was significantly developed, resulting in higher values of the Nusselt number. The maximum values of the Nusselt numbers were 4.9 for the 60 mm sections and 7.1 for the 80 mm sections, occurring at approximately 80 °C. Further increases in the temperature led to a linear decrease in the Nusselt number, which reached around 2 at a temperature of 700 °C for both of the sections.

In the case of the 60 mm section package (Figure 12), the MG_{ETC} parameter increased across the entire temperature range, with the lines illustrating changes in this parameter showing slight fluctuations. For this charge, the convection and conduction in the gas transfer reached a maximum of approximately 5% of the energy, with an average value of about 2.5%. For the 80 mm section package (Figure 13), the MG_{ETC} parameter rose significantly up to about 200 °C, after which its value stabilized until approximately 550 °C. With further increases in the temperature, a decline in this parameter was observed. In this case, the maximum MG_{ETC} value reached around 9%, with the average value stabilizing at about 5%. Table 4 summarizes the minimum, average, and maximum MG_{ETC} values obtained for all the considered cases. To conclude this part of the research, it should be noted that the thermal phenomena occurring in this gas region had a negligible impact on the overall heat transfer during the heating and cooling of the discussed charge. Ignoring these phenomena greatly simplified the mathematical description of the heat exchange process without adversely affecting the accuracy of the obtained results.

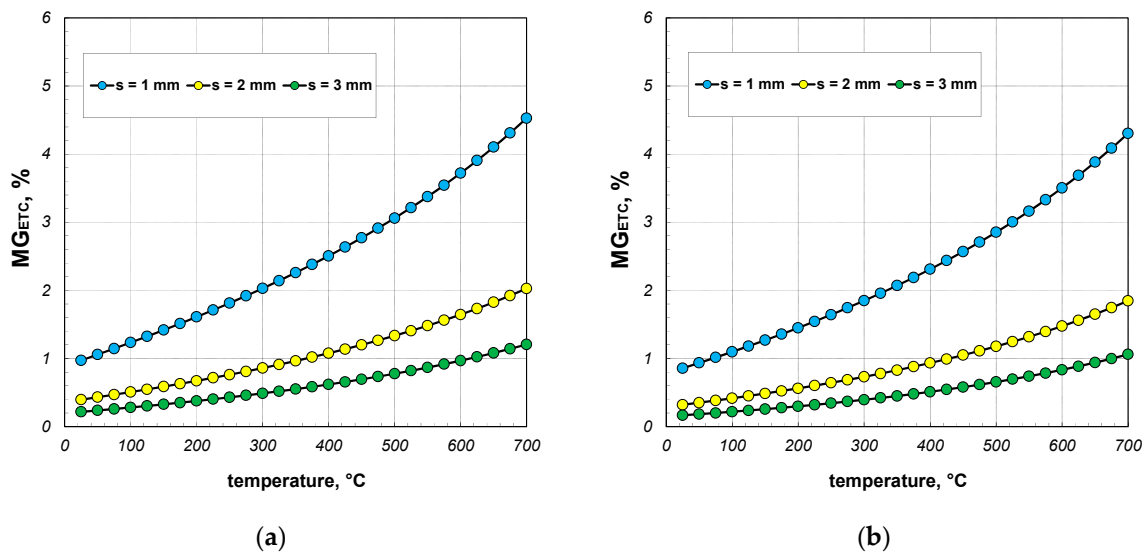


Figure 11. MG_{ETC} parameter of the 40 mm section package for the (a) minimum and (b) maximum joint resistance.

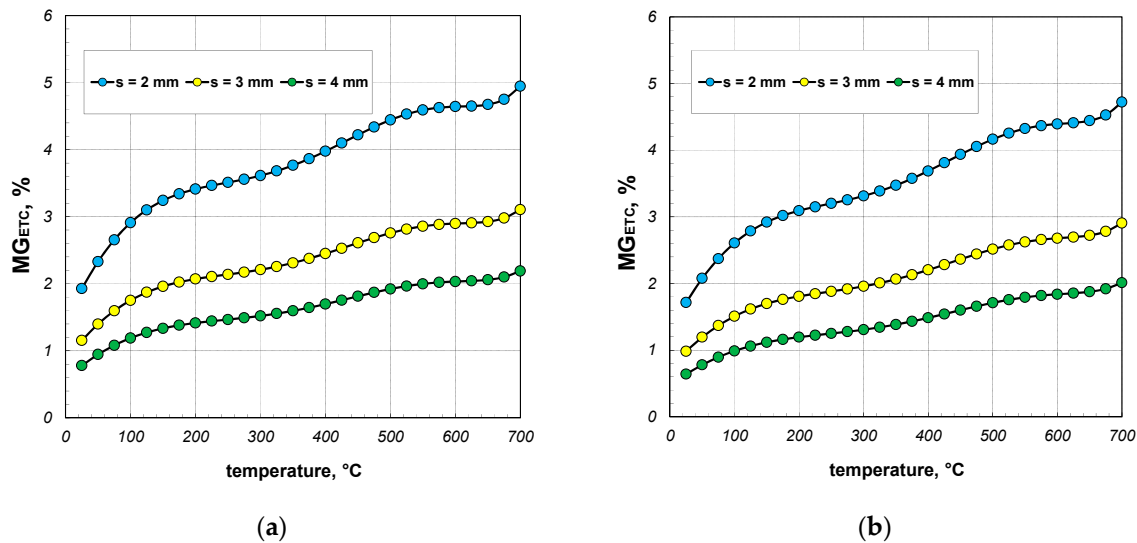


Figure 12. MG_{ETC} parameter of the 60 mm section package for the (a) minimum and (b) maximum gap resistance.

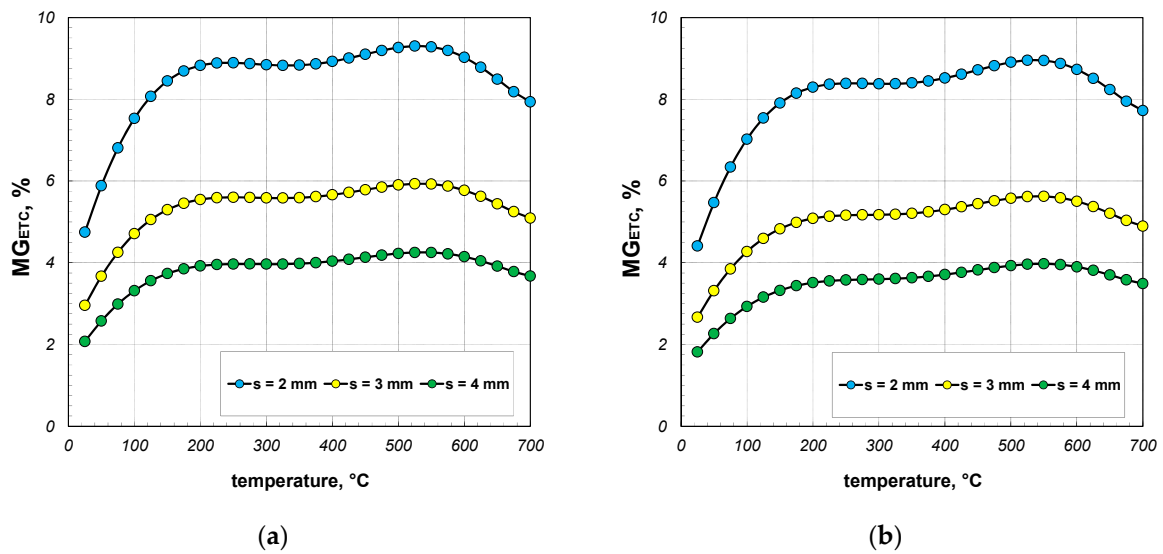


Figure 13. MG_{ETC} parameter of the 80 mm section package obtained for the (a) minimum and (b) maximum gap resistance.

Table 4. The minimum, average, and maximum values of MG_{ETC} parameter.

Section Dimension	Wall Thickness	$MG_{ETC}, \%$					
		R_{gp-min}			R_{gp-max}		
		Min	Mean	Max	Min	Mean	Max
40 mm	1 mm	0.97	2.47	4.53	0.86	2.28	4.30
	2 mm	0.39	1.07	2.03	0.32	0.93	1.85
	3 mm	0.22	0.62	1.21	0.16	0.51	1.06
60 mm	2 mm	1.93	3.82	4.94	1.71	3.53	4.72
	3 mm	1.16	2.35	3.11	0.93	2.11	2.90
	4 mm	0.78	1.63	2.19	0.64	1.42	2.01
80 mm	2 mm	4.75	8.45	9.30	4.41	8.05	8.96
	3 mm	2.96	5.36	5.93	2.66	4.99	5.62
	4 mm	2.07	3.81	4.25	1.82	3.49	3.97

Another step of the quantitative analysis of heat exchange in the section package was to examine the impact of thermal radiation. To analyze this problem, a parameter denoted as MR_{ETC} was defined as follows:

$$MR_{ETC} = \frac{ETC - ETC_{WR}}{ETC_{WR}}, \tag{25}$$

where ETC_{WR} denotes the effective thermal conductivity of the package calculated by neglecting the thermal radiation between the internal surfaces of the section. The value of ETC_{WR} was obtained by excluding the radiation resistance R_{rd} from the computational model.

The results of the calculations for the parameter MR_{ETC} are presented in Figures 14–16. As seen in all the cases, this parameter increased significantly with temperature. This trend arose from the fact that the intensity of the thermal radiation between the internal surfaces of the section was proportional to the third power of their mean absolute temperature. In contrast to the parameter MG_{ETC} , which remained at a few percent, the values of MR_{ETC} significantly exceeded 100%. Up to a temperature of 400 °C, the heating of the package

was primarily driven by heat conduction through the walls of the sections. However, beyond this temperature, thermal radiation became the key phenomenon responsible for the transfer of thermal energy. Thus, when analyzing the heat transfer process in the examined load, neglecting thermal radiation was not an option. The minimum, average, and maximum values of MR_{ETC} obtained for all the analyzed cases are summarized in Table 5.

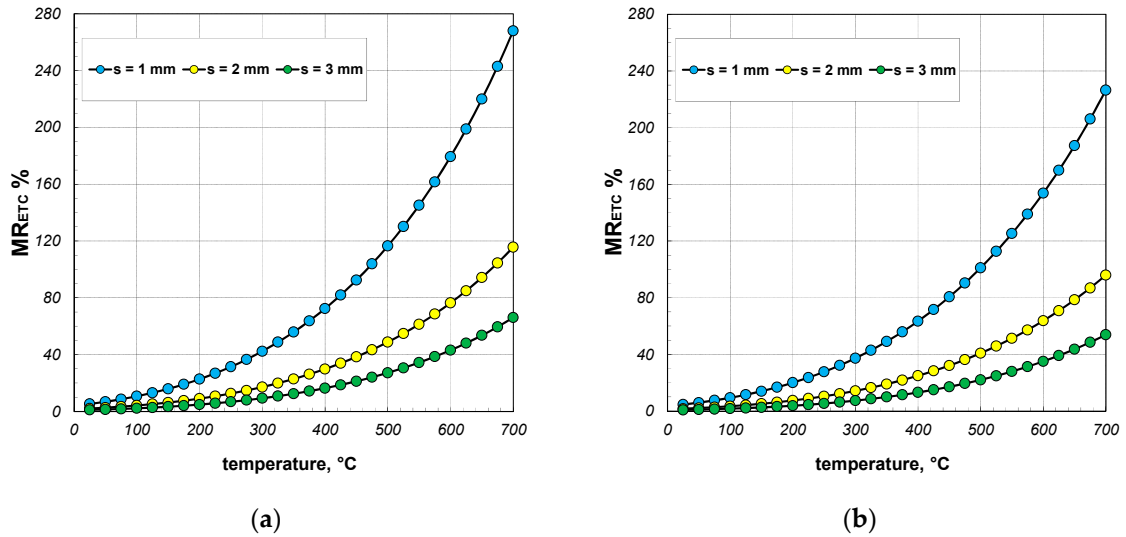


Figure 14. MR_{ETC} parameter of the 40 mm section package for the (a) minimum and (b) maximum gap resistance.

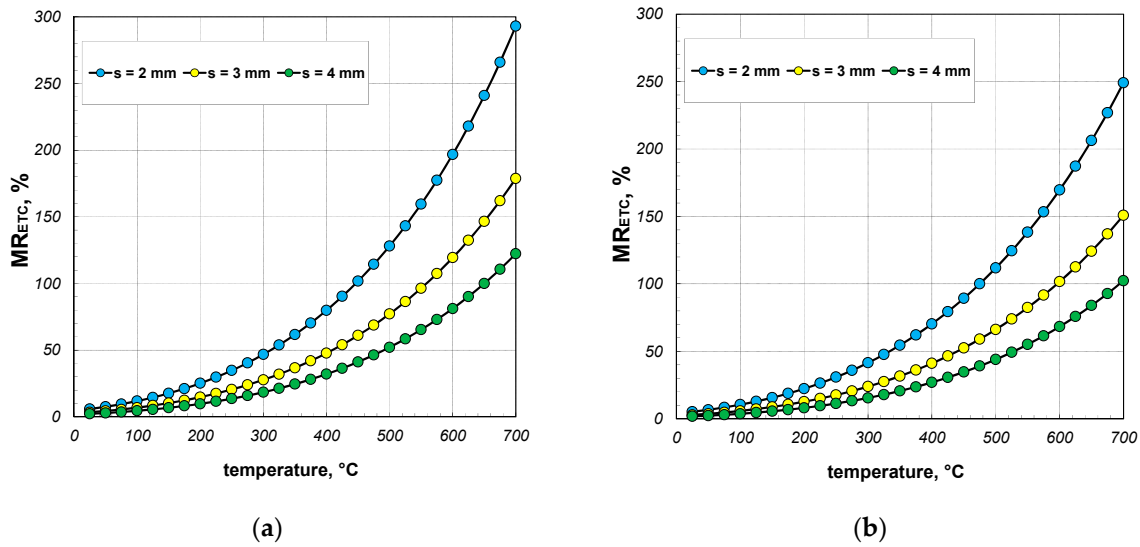


Figure 15. MR_{ETC} parameter of the 60 mm section package for the (a) minimum and (b) maximum gap resistance.

The final element of the analysis presented in this article was to assess the quality of the results from the proposed model. For this purpose, the results of the experimental investigations on the effective thermal conductivity (ETC) of the square section packages were utilized [64]. The samples used in the experiments were constructed from sections made of S235JRH steel grade, which had a maximum carbon content of 0.2% [65]. The measurement results obtained for the 40 mm and 60 mm sections with a wall thickness of 3 mm are shown in Figures 17a and 18a, respectively. These figures also include the model calculation results obtained for the minimum and maximum values of resistance R_j . As can

be seen, in both cases, the measured results were close to the minimum model values. To perform a precise quantitative comparison of the presented results, the measurement data were approximated with regression functions in the form of second-degree polynomials. For the individual sections, these functions are as follows:

$$ETC_{40} = 6.3 \cdot 10^{-7} \cdot t^2 + 0.0024t + 3.89, \tag{26}$$

$$ETC_{60} = 2.3 \cdot 10^{-6} \cdot t^2 + 0.0014t + 4.42. \tag{27}$$

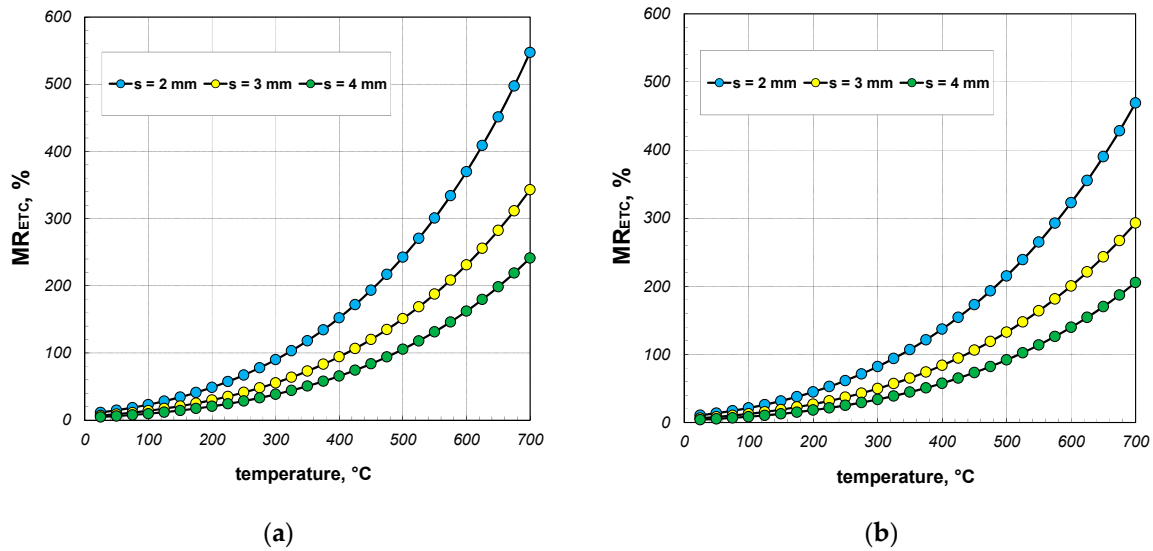


Figure 16. MR_{ETC} parameter of the 80 mm section package for the (a) minimum and (b) maximum gap resistance.

Table 5. The minimum, average, and maximum values of MR_{ETC} parameter.

Section Dimension	Wall Thickness	$MR_{ETC}, \%$					
		R_{gp-min}			R_{gp-max}		
		Min	Mean	Max	Min	Mean	Max
40 mm	1 mm	5.3	79.7	261.9	4.6	74.9	226.5
	2 mm	2.1	33.5	115.5	1.6	30.3	95.9
	3 mm	1.1	20.3	569.6	0.8	16.5	53.8
60 mm	2 mm	5.9	95.1	293.1	5.2	82.3	249.1
	3 mm	3.4	57.3	178.8	2.9	48.9	150.8
	4 mm	2.2	38.8	122.3	1.8	32.6	102.4
80 mm	2 mm	11.6	179.5	547.3	10.7	158.2	469.0
	3 mm	7.1	111.8	342.9	6.3	97.6	292.9
	4 mm	4.8	78.2	241.3	4.2	67.7	205.4

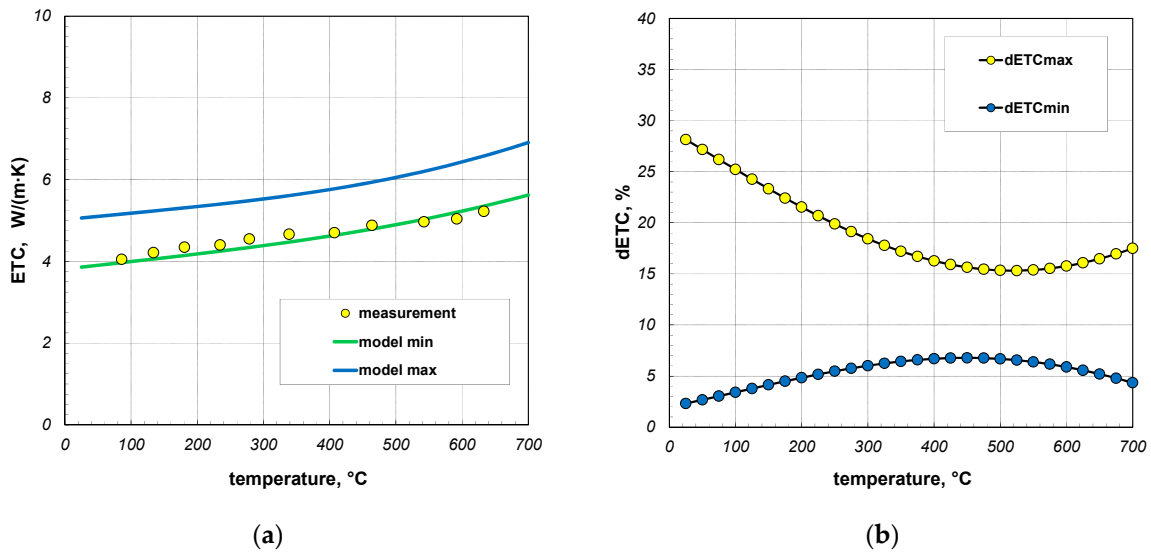


Figure 17. Comparison of measured and model values of ETC for 40 mm sections package (a) and changes in dETC parameter (b); results obtained for emissivity 0.7.

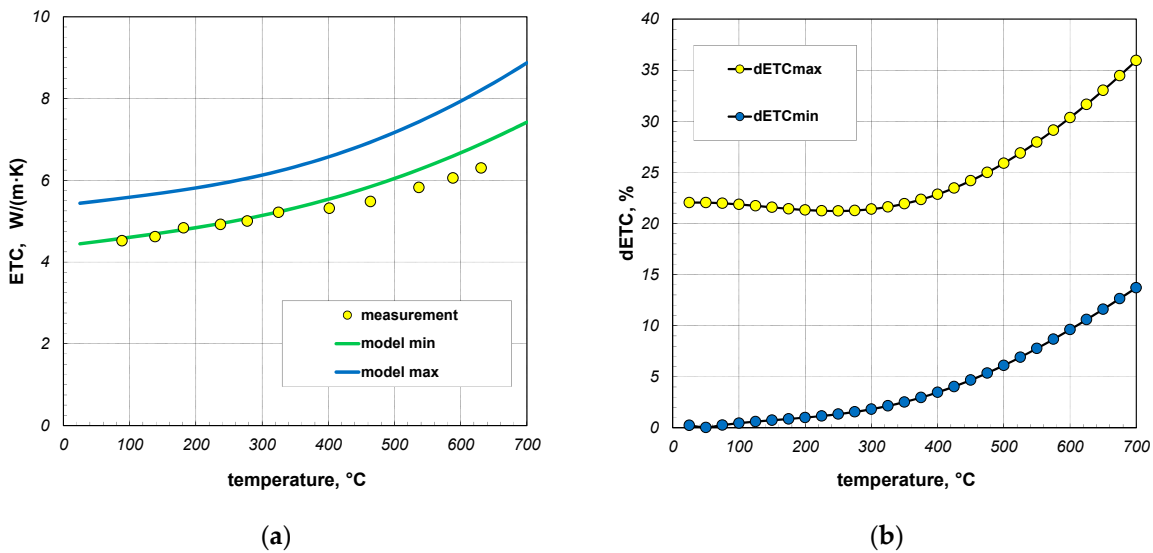


Figure 18. Comparison of measured and model values of ETC for 60 mm sections package (a) and changes in dETC parameter (b); results obtained for emissivity 0.7.

The determination coefficients R_2 for these functions were 0.986 and 0.984, respectively. Values close to unity indicate that the adopted equations are well-fitted to the measurement results.

For further analysis, the parameter dETC was defined using the following equations:

$$dETC_{\max} = \frac{|ETC_{me} - ETC_{\max}|}{ETC_{me}} \cdot 100\% \tag{28}$$

$$dETC_{\min} = \frac{|ETC_{me} - ETC_{\min}|}{ETC_{me}} \cdot 100\% \tag{29}$$

where ETC_{me} —measured values, ETC_{\max} —maximum modeled values, ETC_{\min} —minimum modeled values.

The results of the calculations for the parameter dETC obtained for the analyzed packages are presented in Figures 17b and 18b. For the 40 mm profile package, the average

value of the parameter $dETC_{min}$ was 5.3%, while the maximum value was 6.8%. This indicates a relatively high consistency between the model results and the measurement data. For the parameter $dETC_{max}$, these values were 19.1% and 28.2%, respectively. For the 60 mm profile package, the average and maximum values of $dETC_{min}$ were 4.4% and 13.7%, respectively. For $dETC_{max}$, the values were 24.8% and 35.9%. The presented results demonstrate that when modeling the ETC of the profile package, it was necessary to use Equation (19), which describes the maximum value of this parameter, when addressing the thermal resistance of joints. The ETC values calculated using Equation (18), which described the minimum value of R_j , were overestimated for both profile dimensions.

As shown in Figure 18a, the measurement results and minimum model values were practically coincident up to a temperature of about 350 °C. However, with further increases in temperature, a growing difference was observed, with the model values exceeding the measurement data. Consequently, additional calculations were performed with a reduced emissivity of 0.5. This emissivity was characteristic of cold-rolled steel products with a clean surface [66,67]. The results of these calculations are presented in Figure 19a. In this situation, the model values were slightly lower than the measurement data. Considering that the experimental data were characterized by a measurement uncertainty of 5% [64], it can be concluded that, in this case, a nearly perfect fit had been achieved for the minimum model values. This applies to both the values of ETC and the nature of their changes as a function of temperature. As shown in Figure 19b, the maximum value of the parameter $dETC_{min}$ for this case was 3.8%, with an average value of 2.1%. This was below the measurement uncertainty of the experimental results.

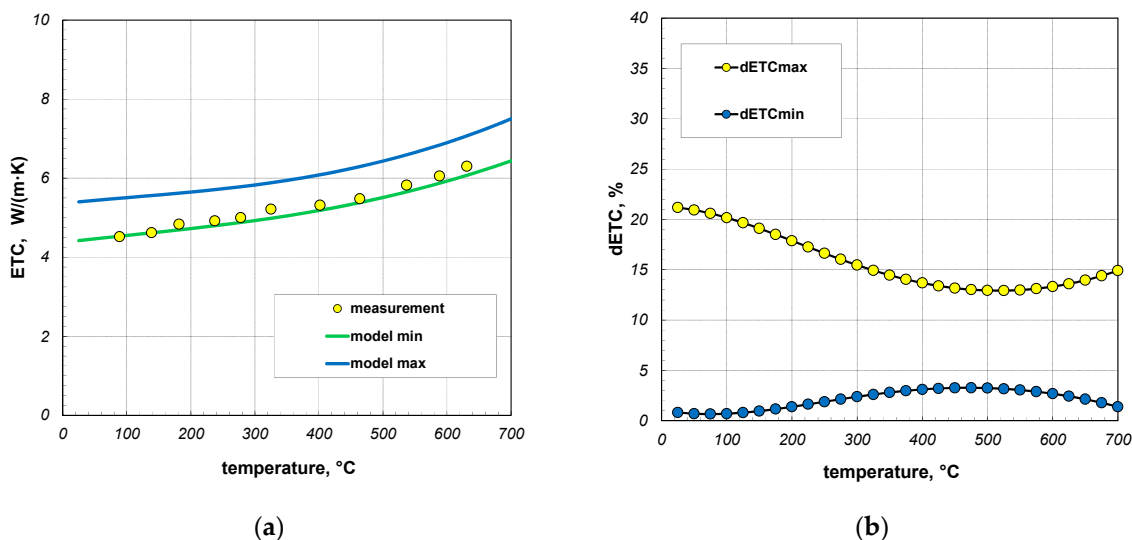


Figure 19. Comparison of measured and model values of ETC for 60 mm sections package (a) and changes in $dETC$ parameter (b); results obtained for emissivity 0.5.

The results presented demonstrate that using the proposed computational model, along with the proper adjustment of the thermophysical parameters, it is possible to accurately replicate the values of the effective thermal conductivity (ETC) of the profile package. Given that the analyzed problem involved a very complex physical phenomenon, the behavior of which depended on a variety of factors, even an adjustment accuracy of several percentage points, as achieved for ETC_{max} , should be considered acceptable.

4. Conclusions

Based on the calculations performed, the following conclusions can be drawn:

- The effective thermal conductivity (ETC) of the package of square steel sections for the considered geometrical cases varied between 2.2 and 10.6 W/(m·K);

- The ETC value of the package was an order of magnitude lower than the thermal conductivity of the individual sections;
- The ETC of the analyzed charge increased dynamically with temperature;
- The ETC increased as a function of the section size and wall thickness;
- Below 350 °C, the primary mechanism governing the heating of the package was heat conduction in the section walls;
- Above 350 °C, the mechanism that determined the heating of the package was thermal radiation;
- The gas convection inside the sections had minimal impact on the heating process of the package;
- The key parameters influencing the quality of the results were the joint resistance between adjacent sections and the emissivity of the sections.

In summary, the presented research emphasizes that the proposed model is universal and allows for the analysis of various geometric configurations related to changes in the dimensions of the profiles, as well as the packing or arrangement of a bundle. However, for a package with different geometry, the form of the individual equations must be modified to account for new geometric parameters. The article only analyzed the impact of wall thickness and the external dimensions of the profiles on heat transfer in a maximally packed bundle, as this type of charge was most commonly subjected to heat treatment. A loosely packed bundle (with higher internal porosity due to the presence of gaps between the profiles) will exhibit a lower value of ETC and, consequently, will heat up more slowly. At the same time, it will occupy more space in the furnace chamber, which should be utilized as efficiently as possible to maximize production process efficiency. For this reason, it is rational to heat only maximally packed bundles.

This model can be applied to a bundle of profiles made from any material. When changing the material, it is only necessary to adjust the equations describing its thermal conductivity (Equation (20)) and the equations describing the resistance R_j (Equations (18) and (19)). However, the validation of the model for a different material requires additional experimental investigations, as the forms of Equations (18) and (19) can only be determined through measurements. This model also allows for the inclusion of the type of atmosphere in which the heat treatment is carried out. The effect of the gas type on heat transfer within the bundle is accounted for by the heat transfer coefficient k_g , which appears in Equation (16). This equation describes the thermal resistance in the gas region. In the simplest case, one value can be provided, e.g., 0.024 W/(m·K)—the value for air at room temperature. In a more precise solution, a dependence describing the changes in this parameter as a function of temperature should be provided. This was also the approach taken during the calculations, where the change in air thermal conductivity as a function of temperature was described using a second-degree polynomial—Equation (21). Changing the type of gas in the model calculations requires only modifying one equation. The form of this equation, describing the temperature dependence of the thermal conductivity of a specific gas, can be determined by approximating the literature data. For example, if the heat treatment is conducted in a hydrogen atmosphere, which is often encountered in industrial practice [8,27], the coefficient k_g should be described by the following equation:

$$k_g = 0.0004 t + 0.184. \quad (30)$$

In special cases, the heat treatment of steel products is conducted in vacuum furnaces [68,69]. The use of a vacuum offers several advantages, including the elimination of surface oxidation of the heated elements [70]. In the analysis of heat treatment in a vacuum furnace, the resistance R_g described by Equation (16) should be omitted from the model. The impact of the gas type, or the absence of gas, on the heat transfer process within the bundle is an interesting problem and will undoubtedly be the subject of analysis in future publications.

As mentioned in the introduction, computer programs utilizing numerical algorithms are currently employed to control heat treatment processes. The presented model can be implemented as one of the procedures within such a program. The ability to accurately determine the thermophysical properties of the heated package provided by this model is crucial for optimizing the industrial heat treatment of steel sections.

Author Contributions: Conceptualization, R.W. and S.G.A.; methodology, R.W. and V.B.; formal analysis, R.W., V.B. and M.G.; writing—original draft preparation, R.W., V.B. and G.A.V.; visualization, M.G. and G.A.V.; supervision, V.B. and S.G.A. All authors have read and agreed to the published version of the manuscript.

Funding: This research received no external funding.

Institutional Review Board Statement: Not applicable.

Informed Consent Statement: Not applicable.

Data Availability Statement: The original contributions presented in this study are included in the article. Further inquiries can be directed to the corresponding author.

Conflicts of Interest: The authors declare no conflicts of interest.

References

1. Kwon, W.H.; Choi, S.W.; Lee, E.B. Development of Cycloid-Shaped Roll Charging Chute for Sintering Process for Energy Decarbonization and Productivity Improvement in Steel Plants. *Energies* **2024**, *17*, 1536. [[CrossRef](#)]
2. Bataille, C.; Melton, N. Energy efficiency and economic growth: A retrospective CGE analysis for Canada from 2002 to 2012. *Energy Econ.* **2017**, *64*, 118–130. [[CrossRef](#)]
3. Baig, A.A.; Fung, A.S.; Kumar, R. Auditing and Analysis of Natural Gas Consumptions in Small- and Medium-Sized Industrial Facilities in the Greater Toronto Area for Energy Conservation Opportunities. *Energies* **2024**, *17*, 1744. [[CrossRef](#)]
4. Tahmasebi, M.M.; Banihashemi, S.; Hassanabadi, M.S. Assessment of the Variation Impacts on Windwos on Energy Consumption and Carbon Footprint. *Procedia Eng.* **2011**, *21*, 820–828. [[CrossRef](#)]
5. Górecki, J.; Berdychowski, M.; Gawrońska, E.; Wałęsa, K. Influence of PPD and Mass Scaling Parameter on the Goodness of Fit of Dry Ice Compaction Curve Obtained in Numerical Simulations Utilizing Smoothed Particle Method (SPH) for Improving the Energy Efficiency of Dry Ice Compaction Process. *Energies* **2023**, *16*, 7194. [[CrossRef](#)]
6. Lohri, C.; Rajabu, H.; Sweeney, D.; Zurbrugg, C. Char fuel production in developing countries—A review of urban biowaste carbonization. *Renew. Sustain. Energy Rev.* **2016**, *59*, 1514–1530.
7. Sahay, S.S.; Krishnan, K.; Kuthle, M.; Chodha, A.; Bhattacharya, A.; Das, A.K. Model-Based Optimization of a Highly Automated Industrial Batch Annealing Operation. *Iron. Steel.* **2006**, *33*, 306–314. [[CrossRef](#)]
8. Saboonchi, A.; Hassanpour, S. Simulation of Cold Rolled Steel Coil Heating during Batch Annealing Process. *Heat Trans. Eng.* **2008**, *29*, 893–901. [[CrossRef](#)]
9. Sahay, S.S.; Kumar, A.M.; Chatterjee, A. Development of integrated model for batch annealing of cold rolled steels. *Iron. Steel.* **2004**, *31*, 144–152. [[CrossRef](#)]
10. Mathotra, C.P.; Pedenekar, N.R.; Sahay, S.S. Cost model for the steel reheating operation. *Ind. Heat.* **2002**, *69*, 67–71.
11. Sahay, S.S.; Mitra, K. Cost model-based optimization of carburizing operation. *Surf. Eng.* **2004**, *20*, 379–384. [[CrossRef](#)]
12. Kotrbacek, P.; Chabicosky, M.; Resl, O.; Kominek, J.; Luks, T. The Efficient Way to Design Cooling Sections for Heat Treatment of Long Steel Products. *Materials* **2023**, *16*, 3983. [[CrossRef](#)] [[PubMed](#)]
13. Zhang, Z.; Roberts, S.; Wildgoose, J.; Philpott, W.; Jepson, M.A. Effects of post-weld heat treatment on the microstructure and properties of the matching SMAW filler metal for weld joints in MarBN steel. *Weld World* **2024**, *68*, 1549–1561. [[CrossRef](#)]
14. Kulkarni, A.R.; Raju, P.V.; Sarma, P.P.; Dewangan, S.; Selvaraj, S.K. Microstructure and Mechanical Properties of 0.18%-C Steel Samples Processed Through Five Different Heat Treatment Techniques. *J. Inst. Eng. India Ser. D* **2024**. [[CrossRef](#)]
15. Shi, F.; Zheng, J.; Zhang, J.; Zhao, Y.; Chen, L. Heat Treatment Process, Microstructure, and Mechanical Properties of Spring Steel with Ultra-High Strength and Toughness. *Metals* **2024**, *14*, 180. [[CrossRef](#)]
16. Meshkabadi, R.; Pouyafar, V.; Soltanikia, R. Investigation on Microstructure, Hardness and Fracture Energy of AISI H13 Hot Work Tool Steel by Cyclic Heat Treatment. *J. Mater. Eng. Perform.* **2024**, *33*, 6620–6629. [[CrossRef](#)]
17. Talebi, F.; Jamaati, R.; Hosseinipour, S.J. Strong strain-hardening capability in plain carbon steel through cold rolling and heat treatment of lamellar structure. *Arch. Civ. Mech. Eng.* **2024**, *24*, 44. [[CrossRef](#)]
18. Jaluria, Y. Numerical simulation of the transport process in a heat treatment furnace. *Int. J. Num. Meth. Eng.* **1988**, *25*, 387–399. [[CrossRef](#)]
19. Rao, T.R.; Barth, G.J.; Miller, J.R. Computer model prediction of heating, soaking and cooking times in batch coil annealing. *Iron Steel Eng.* **1983**, *60*, 22–33.
20. Laden, B. A control system for fuel optimization reheating furnaces. *Scand. J. Metall.* **1986**, *15*, 16–24.

21. Musiał, D. Numerical analysis of the process of heating of a bed of steel bars. *Arch. Met. Mater.* **2013**, *58*, 63–66. [[CrossRef](#)]
22. Kolmasiak, C.; Wyleciał, T. Heat treatment of steel products as an example of transport phenomenon in porous media. *Metalurgija* **2018**, *57*, 363–366.
23. Sahay, S.S.; Krishnan, K. Model based optimization of continuous annealing operation for bundle of packed rods. *Iron. Steel.* **2007**, *34*, 89–94. [[CrossRef](#)]
24. Zhao, C.Y.; Lu, T.J.; Hudson, H.P.; Jackson, J.D. The temperature dependence of effective thermal conductivity of open-celled steel alloy foams. *Mater. Sci. Eng. A* **2004**, *367*, 123–131. [[CrossRef](#)]
25. Öchsner, A.; Murcg, G.E.; de Lemos, M.J.S. (Eds.) *Cellular and Porous Materials: Thermal Properties Simulation and Prediction*; WILEY-VCH Verlag GmbH & Co., KGaA: Weinheim, Germany, 2008.
26. Van Antwerpen, W.; du Toit, C.G.; Rousseau, P.G. Review of Correlations to Model the Packing Structure and Effective Thermal Conductivity in Packed Beds of Mono-Sized Spherical Particles. *Nucl. Eng. Des.* **2010**, *240*, 1803–1818. [[CrossRef](#)]
27. Zuo, Y.; Wu, W.; Zhang, X.; Lin, L.; Xiang, S.; Liu, T.; Niu, L.; Huang, X. A study of heat transfer in high-performance hydrogen bell-type annealing furnace. *Heat Trans. Asian Res.* **2001**, *30*, 615–623. [[CrossRef](#)]
28. Zhang, X.; Yu, F.; Wu, W.; Zuo, Y. Application of radial effective thermal conductivity for heat transfer model of steel coils in HPH furnace. *Int. J. Ther.* **2003**, *24*, 1395–1405. [[CrossRef](#)]
29. ASTM C1044-12; Standard Practice for Using a Guarded-Hot-Plate Apparatus or Thin-Heater Apparatus in the Single-Sided Mode. ASTM International: West Conshohocken, PA, USA, 2012.
30. ASTM C177-13; Standard Test Method for Steady-State Heat Flux Measurements and Thermal Transmission Properties by Means of the Guarded-Hot-Plate Apparatus. ASTM International: West Conshohocken, PA, USA, 2013.
31. Carson, J.K. Review of Effective Thermal Conductivity Models for Foods. *Int. J. Refrig.* **2006**, *29*, 958–967. [[CrossRef](#)]
32. Carson, J.K.; Lovatt, S.J.; Tanner, D.J.; Cleland, A.C. Thermal conductivity bounds for isotropic, porous materials. *Int. J. Heat Mass Trans.* **2005**, *48*, 2150–2158. [[CrossRef](#)]
33. Horai, K. Thermal Conductivity of Hawaiian Basalt: A New Interpretation of Robertson and Peck's Data. *J. Geophys. Res.* **1991**, *96*, 4125–4132. [[CrossRef](#)]
34. Beck, J.M.; Beck, A.E. Computing Thermal Conductivities of Rocks from Chips and Conventional Specimen. *J. Geophys. Res.* **1965**, *70*, 5227–5239. [[CrossRef](#)]
35. Krischer, O. *Die Wissenschaftlichen Grundlagen der Trocknungstechnik*; Springer: Berlin, Germany, 1963. (In German)
36. Woodside, W.; Messmer, J. Thermal Conductivity of Porous Media, I: Unconsolidated Sands and II: Consolidated Sands. *J. Appl. Phys.* **1961**, *32*, 1688–1768. [[CrossRef](#)]
37. Assad, A. *Study of Thermal Conductivity of Fluid Bearing Porous Rocks*; University of California: Berkeley, CA, USA, 1955.
38. Abareshi, M.; Youssefi, A. Fabrication, Characterization and Measurement of Thermal Conductivity of Fe₃O₄ Nanofluids. *J. Magn. Magn. Mat.* **2010**, *322*, 3895–3901. [[CrossRef](#)]
39. Wyczółkowski, R.; Benduch, A. The Possibilities of Determining the Effective Thermal Conductivity of Steel Rectangular Section Bundles Based on the Selected Literature Models. *J. Phys. Sci. App.* **2016**, *6*, 48–58. [[CrossRef](#)]
40. Wyczółkowski, R.; Bagdasaryan, V.; Gała, M. Experimental Investigation of Thermal Contact Conductance in a Bundle of Flat Steel Bars. *Appl. Sci.* **2022**, *12*, 6977. [[CrossRef](#)]
41. Wyczółkowski, R.; Musiał, D. The experimental study of natural convection within the space of a bundle of rectangular sections. *Exp. Therm. Fluid Sci.* **2013**, *51*, 122–134. [[CrossRef](#)]
42. Wyczółkowski, R. Analysis of the Rayleigh number in the area of steel rectangular sections in the conditions of steady and unsteady heat flow. *Civ. Environ. Eng. Rep.* **2014**, *14*, 107–118.
43. Wyczółkowski, R.; Szmidla, J.; Gała, M.; Bagdasaryan, V. Analysis of Nusselt Number for Natural Convection in Package of Square Steel Sections. *Acta Phys. Pol. A* **2020**, *139*, 548–551. [[CrossRef](#)]
44. Cengel, Y.A. *Heat and Mass Transfer—A Practical Approach*, 3rd ed.; Mc Graw Hill: New York, NY, USA, 2007.
45. Islam, M.R.; Pramila, A. Thermal conductivity of fibre reinforced composites by the FEM. *J. Compos. Mater.* **1999**, *33*, 1699–1715. [[CrossRef](#)]
46. Bakker, K. Using the finite element method to compute the influence of complex porosity and inclusion structures on the thermal and electrical conductivity. *Int. J. Heat Mass Transf.* **1997**, *40*, 3503–3511. [[CrossRef](#)]
47. Thovert, J.F.; Wary, F.; Adler, P.M. Thermal conductivity of random media and regular fractals. *J. App. Phys.* **1990**, *68*, 3872–3883. [[CrossRef](#)]
48. Veyret, D.; Cioulachtjian, L.; Tadrist, L.; Pantaloni, J. Effective thermal conductivity of a composite material: A numerical approach. *J. Heat Transfer.* **1993**, *115*, 866–871. [[CrossRef](#)]
49. Tian, W.X.; Zhang, K.; Hou, Y.D.; Zhang, Y.P.; Qiu, S.Z.; Su, G.H. Hydrodynamics of two-phase flow in a rod bundle under cross-flow condition. *Ann. Nucl. Energy* **2016**, *91*, 206–214. [[CrossRef](#)]
50. Faraji, H.; Tegger, M.; Arshad, A.; Arıcı, M.; Mehdi Berra, E.; Choukairy, K. Lattice Boltzmann simulation of natural convection heat transfer phenomenon for thermal management of multiple electronic components. *Ther. Sci. Eng. Prog.* **2023**, *45*, 102126. [[CrossRef](#)]
51. Afaynou, I.; Faraji, H.; Choukairy, K.; Arıcı, M.; Khallaki, K. Heat transfer improvement of phase change materials by metal foams and nanoparticles for efficient electronic thermal management: A comprehensive study. *Int. J. Heat Mass Transf.* **2024**, *227*, 125534. [[CrossRef](#)]

52. Sohag, F.A.; Mohanta, L.; Cheung, F.B. CFD analyses of mixed and forced convection in a heated vertical rod bundle. *App. Therm. Eng.* **2017**, *117*, 85–93. [CrossRef]
53. Nellis, G.; Klein, S. *Heat Transfer*; Cambridge University Press: New York, NY, USA, 2012.
54. Kostowski, E. *Heat Flow*; Wydawnictwo Politechniki Śląskiej: Gliwice, Poland, 2000. (In Polish)
55. Modest, M.F. Chapter 5. Radiative Exchange Between Gray, Diffuse Surfaces. In *Radiative Heat Transfer*, 3rd ed.; Academic Press: New York, NY, USA; San Francisco, CA, USA; London, UK, 2013; pp. 160–198.
56. Wyczółkowski, R. Computational model of complex heat flow in the area of steel rectangular section. *Procedia Eng.* **2016**, *157*, 185–192. [CrossRef]
57. Yovanovich, M.M.; Marotta, E.E. Chapter 4. Thermal spreading and contact resistances. In *Heat Transfer Handbook*; Bejan, A., Kraus, A.D., Eds.; John Wiley & Sons, Inc.: New York, NY, USA, 2003.
58. Yovanovich, M.M. Four decades of research on thermal contact, gap, and joint resistances in microelectronics. *IEEE Trans. Comp. Pack. Technol.* **2005**, *20*, 182–206. [CrossRef]
59. Furmański, P.; Wiśniewski, T.S.; Banaszek, J. *Thermal Contact Resistances and Other Thermal Phenomena at Solid-Solid Interface*; Institute of Heat Engineering—Warsaw University of Technology: Warsaw, Poland, 2008.
60. Sridhar, M.R.; Yovanovich, M.M. Review of elastic and plastic contact conductance models: Comparison with experiment. *J. Thermophys. Heat Transf.* **1994**, *8*, 633–640. [CrossRef]
61. Liščić, B. *Steel Heat Treatment—Metallurgy and Technologies*; CRC Taylor & Francis Group: Boca Raton, FL, USA; London, UK; New York, NY, USA, 2006.
62. Wyczółkowski, R.; Strycharska, D.; Bagdasaryan, V. Correlations for the thermal conductivity of selected steel grades as a function of temperature in the range of 0–800 °C. *Arch. Thermod.* **2022**, *43*, 29–45.
63. Ražnjević, K. *Thermal Table with Diagrams*; WNT: Warsaw, Poland, 1966. (In Polish)
64. Wyczółkowski, R. Experimental Investigations of Effective Thermal Conductivity of the Selected Examples of Steel Porous Charge. *Solids* **2021**, *2*, 420–436. [CrossRef]
65. European Steel and Alloy Grades/Numbers Steel Number. Available online: http://www.steelnumber.com/en/steel_composition_eu.php?name_id=645 (accessed on 25 October 2024).
66. Emissivity—Metals. Available online: <https://www.flukeprocessinstruments.com/en-us/service-and-support/knowledge-center/infrared-technology/emissivity-metals> (accessed on 25 October 2024).
67. Emissivity_Table. Available online: https://www.transmetra.ch/images/transmetra_pdf/publikationen_literatur/pyrometrie-thermografie/emissivity_table.pdf (accessed on 25 October 2024).
68. TDMAW_SOS_Spring_Page_Kinetic_Vacuum_Heat_Treat_Article. Available online: https://knifemaker.com/wp-content/uploads/2020/11/TDMAW_SOS_Spring_Page_Kinetic_Vacuum_Heat_Treat_Article.pdf (accessed on 25 October 2024).
69. Heat Treatment-Vacuum-What Is It? Available online: <https://polmet.zagan.pl/en/blog/31-heat-treatment-vacuum-what-is-it> (accessed on 25 October 2024).
70. Why Vacuum Heat Treatment Is a Good Idea. Available online: <https://www.miheuprecision.com/blog/vacuum-heat-treatment> (accessed on 25 October 2024).

Disclaimer/Publisher’s Note: The statements, opinions and data contained in all publications are solely those of the individual author(s) and contributor(s) and not of MDPI and/or the editor(s). MDPI and/or the editor(s) disclaim responsibility for any injury to people or property resulting from any ideas, methods, instructions or products referred to in the content.